Digital Predistortion for Joint Mitigation of I/Q Imbalance and MIMO Power Amplifier Distortion

Zain Ahmed Khan, *Student Member, IEEE*, Efrain Zenteno, *Member, IEEE*, Peter Händel, *Senior Member, IEEE*, and Magnus Isaksson, *Senior Member, IEEE*

***Abstract*— This paper analyzes the joint effects of in-phase and quadrature (I/Q) imbalance and power amplifier (PA) distortion for RF multiple input multiple output (MIMO) transmitters in the presence of crosstalk. This paper proposes candidate models for the digital predistortion of static I/Q imbalanced sources exciting a dynamic MIMO Volterra system. The proposed models are enhanced using a novel technique based on subsample resolution to account for dynamic I/Q imbalance distortions. Finally, the computational complexity of the proposed models is analyzed for implementation suitability in digital platforms. It is shown that the error spectrum for the proposed models in subsample resolution reaches the noise floor of the measurements. The proposed models achieve a normalized mean squared error of −50 dB and an adjacent channel power ratio of −57 dB for signal bandwidths upto 65 MHz and crosstalk levels ranging to −10 dB. These results demonstrate the effectiveness of the proposed techniques in the joint mitigation of I/Q imbalance and PA distortion with crosstalk for a typical 2 × 2 MIMO telecommunication setup.**

***Index Terms*— Digital predistortion (DPD), in-phase and quadrature (I/Q) imbalance, linearization, multiple input multiple output (MIMO), power amplifier (PA).**

I. Introduction

RF multiple input multiple output (MIMO) transmitters are an emerging candidate technology for coping with increasing data rate demands in wireless communications [1], [2]. A low-cost and energy-efficient transmitter is essential to practical implementation of MIMO systems. However, these requirements result in hardware impairments, which degrade the data rate capacity deteriorating the system performance [3].

Contemporary RF transmitters are composed of analog and digital stages that complement each other. Typically, the RF analog side is enhanced with digital techniques [4]. These digital techniques compensate for the distortions present at the modulation and amplification stages of the RF transmitter. The distortion in the former stage is dominated by in-phase and quadrature (I/Q) imbalance effects [5]–[7] and in the latter by nonlinear effects [8]. The nonlinear distortions are compensated with the widely studied digital predistortion (DPD) method [9]–[11], where the complex-valued baseband input signal is preprocessed, such that the output of the power amplifier (PA) is linearized. However, I/Q imbalance impairments introduce additional in-band and out of band distortions at the PA output as well as degrade the DPD performance [12], [13]. Methods that mitigate I/Q imbalance and PA nonlinearity separately [13]–[15] suffer from additional RF hardware requirements. Hence, joint schemes that compensate for I/Q imbalance and PA nonlinearity become significant.

Joint effects of I/Q imbalanced sources exciting PAs (modeled as Volterra systems) have been studied extensively for single input single output (SISO) transmitters along with their corresponding compensation techniques, such as [16]–[26]. In this context, frequency-independent (referred to as static) I/Q imbalance impairments are analyzed in [16]–[19], whereas frequency-dependent (referred to as dynamic) I/Q imbalance impairments are considered in [20]–[26]. It should be noted that dynamic I/Q imbalance can be compensated in either time or frequency domains. Time domain compensation techniques are presented in [20]–[23], whereas frequency domain compensation techniques are presented in [24]–[26].

Transitioning to RF MIMO transmitters results in additional hardware impairments, such as RF leakage effects (referred to as crosstalk) between the different transmission paths when being implemented on the same chipset [27]–[30]. Input crosstalk refers to RF leakage prior to the amplification stage, whereas output crosstalk refers to RF leakage after the amplification [31]–[34]. Therefore, to mitigate spectral regrowth, MIMO DPD structures should compensate for the dynamic nonlinear PA distortions as well as both input and output crosstalk jointly at the transmitter. These joint effects are referred to as MIMO PA distortions in this paper.

DPD structures for MIMO PA distortions have been proposed in [31]–[35] without considering I/Q imbalance effects. Similarly, numerous I/Q imbalance compensation techniques

Manuscript received May 13, 2016; revised September 22, 2016; accepted September 23, 2016. Date of publication October 19, 2016; date of current version January 26, 2017.

Z. A. Khan is with the Department of Electronics, Mathematics, and Natural Sciences, University of Gävle, SE 80176 Gävle, Sweden, and also with the Department of Signal Processing, KTH Royal Institute of Technology, SE-100 44 Stockholm, Sweden (e-mail: zakh@kth.se).

E. Zenteno is with the Electronics and Telecommunications Department, Universidad Catolica San Pablo, Arequipa, Peru (e-mail: ezenteno@ucsp.edu.pe).

P. Händel is with the Department of Signal Processing, KTH Royal Institute of Technology, SE-100 44 Stockholm, Sweden (e-mail: ph@kth.se).

M. Isaksson is with the Department of Electronics, Mathematics, and Natural Sciences, the University of Gävle, SE 80176 Gävle, Sweden (e-mail: min@hig.se).

Color versions of one or more of the figures in this paper are available online at http://ieeexplore.ieee.org.

Digital Object Identifier 10.1109/TMTT.2016.2614933

0018-9480 © 2016 IEEE. Translations and content mining are permitted for academic research only. Personal use is also permitted, but republication/redistribution requires IEEE permission. See http://www.ieee.org/publications_standards/publications/rights/index.html for more information.

have been developed for MIMO systems [36]–[40] without considering nonlinear PA distortions and crosstalk.

Therefore, this paper is motivated by the study of independent I/Q-impaired sources exciting an MIMO PA foreseen for efficient RF MIMO transmitters [27]–[30]. Therefore, this paper studies joint static IQ imbalance and static MIMO PA distortions for developing effective digital compensation techniques in Section II.

Accordingly, Section III of this paper proposes candidate models for joint mitigation of static I/Q imbalance and MIMO PA distortion at the transmitter inspired by the SISO techniques presented in [20] and [21]. Joint I/Q imbalance and PA distortions in SISO transmitters are compensated using a modeling approach in [20], which deals with imbalances between the I/Q branches separately, whereas augmented conjugate basis functions are used in [21]. These techniques are transformed in conjunction with the MIMO memory polynomial (MP) model [32] yielding the models presented in this paper.

This paper proposes a novel technique based on multirate processing to compensate for dynamic I/Q imbalance effects in Section IV. These effects can be represented as a magnitude and phase difference between the I/Q paths [24], [41], [42]. Therefore, the proposed models are augmented with subsample resolution basis functions to mitigate dynamic I/Q imbalances. Furthermore, the multiple I/Q paths in MIMO systems may suffer time misalignments between them as well, which is tackled simultaneously by the subsample resolution basis.

The proposed techniques are experimentally investigated with crosstalk levels ranging from -40 to -10 dB and signal bandwidths from 4 to 65 MHz in Section V. The error observed for the proposed models augmented with subsampling method is nearly on the noise floor of the measurements demonstrating their effectiveness for the joint mitigation of I/Q imbalance and MIMO PA distortion with marginal increase in complexity. Finally, the proposed models proposed in this paper are shaped to alleviate their computational complexity in Section VI, paving the way for their implementation in resource constrained scenarios.

II. Joint Static I/Q Imbalance and Static MIMO PA Distortion

This section describes static I/Q imbalanced sources exciting a static nonlinear MIMO Volterra series [31], as shown in Fig. 1. It is presented as an example to demonstrate the joint effect of I/Q imbalance on nonlinear PA distortions with crosstalk in the context of an MIMO transmitter. Based on this analysis, candidate mitigation models for joint static I/Q imbalance and dynamic MIMO PA distortion will be proposed in Section III, which would be enhanced for mitigating dynamic I/Q imbalance in Section IV.

For a $K \times K$ MIMO transmitter, let $u_k(t)$ denote the kth carrier continuous time input signal at an instant t, where $k = 1, 2, \ldots, K$. It must be noted that the signals in this paper will be considered in their complex-valued baseband form. The corresponding nth sample of the discrete time input signal, $u_k(n) = u_k(nT_s)$, where $n = 1, 2, \ldots, N$ and T_s is the sampling interval. For simplicity, $u_k(n)$ will be denoted as u_k in this section. The kth complex-valued baseband input signal impaired by static I/Q imbalance, resulting in $\tilde{u}_k$, can be described as [43]

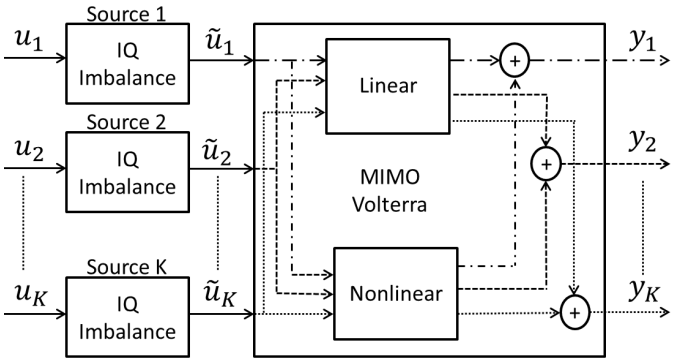

Fig. 1. K I/Q imbalanced sources exciting a static MIMO Volterra system.

$$\tilde{u}_k = \left(a_k u_k + b_k u_k^*\right) \tag{1}$$

where

$$a_k = \cos\left(\frac{\theta_k}{2}\right) + j\alpha_k \sin\left(\frac{\theta_k}{2}\right)$$
$$b_k = \alpha_k \cos\left(\frac{\theta_k}{2}\right) + j \sin\left(\frac{\theta_k}{2}\right). \tag{2}$$

In (2), α_k and θ_k mimic the kth real-valued static (constant) amplitude and phase imbalance terms, respectively. It can be noted that $\tilde{u}_k$ is the sum of the desired baseband signal u_k and its image interference signal u_k^*, where * denotes the complex conjugate operator. The complex-valued coefficients, a_k and b_k, denote the corresponding I/Q imbalance effects described in terms of the image rejection ratio (IRR) denoted by Γ_k. IRR is defined as the power ratio of the image interference signal to the desired baseband signal [24], i.e., for the kth carrier signal, $\Gamma_k = 20\log_{10}|\gamma_k|$, where $\gamma_k = b_k/a_k$. Practical values for the IRR in RF transmitters range from -40 to -20 dB [20]. Finally, in order to capture relative effects between independent sources, a complex-valued gain ζ_k is introduced in (1) as

$$\tilde{u}_k = \zeta_k \left(a_k u_k + b_k u_k^*\right). \tag{3}$$

To study the effects of joint I/Q imbalance and MIMO PA distortion, the set of $\{u_k\}_{k=1}^K$ in (3) is forwarded to a static third-order MIMO Volterra series, as shown in Fig. 1. The resulting ith output for a 2×2 MIMO transmitter is

$$y_i = \sum_{k=1}^{2} h_k^{(i)} \tilde{u}_k + \sum_{k_1=1}^{2}\sum_{k_2=1}^{2}\sum_{k_3=1}^{2} h_{k_1,k_2,k_3}^{(i)}\ \tilde{u}_{k_1}\tilde{u}_{k_2}\tilde{u}_{k_3}^* \tag{4}$$

where the coefficients $h_k^{(i)}$ and $h_{k_1,k_2,k_3}^{(i)}$ describe the linear and third-order nonlinear distortions for an MIMO PA.

From the symmetry property of nonlinear MIMO Volterra, the term $\tilde{u}_1\tilde{u}_2\tilde{u}_1^*$ is the same as $\tilde{u}_2\tilde{u}_1\tilde{u}_1^*$ [34], [44]. This property is used to group equal terms reducing the number of unknown coefficients in (4) resulting in the following

symmetric model:

$$y_i = \sum_{k=1}^{2} h_k^{(i)} \tilde{u}_k + \sum_{k_1=1}^{2} \sum_{k_2=1}^{2} h_{k_1,k_2,k_2}^{(i)} \; \tilde{u}_{k_1} \left|\tilde{u}_{k_2}\right|^2 + \sum_{k_1=1}^{2} \sum_{\substack{k_2=1 \\ k_2 \neq k_1}}^{2} h_{k_1,k_1,k_2}^{(i)} \; \tilde{u}_{k_1}^2 \tilde{u}_{k_2}^*. \tag{5}$$

By inserting (3) in (5)

$$\begin{aligned} y_i = & \sum_{k=1}^{2} \acute{h}_k^{(i)} \left(u_k + \gamma_k u_k^*\right) \\ & + \sum_{k_1=1}^{2} \sum_{k_2=1}^{2} \acute{h}_{k_1,k_2,k_2}^{(i)} \big[u_{k_1} \left|u_{k_2}\right|^2 + \gamma_{k_1} u_{k_1}^* \left|u_{k_2}\right|^2 \\ & \qquad + \gamma_{k_2}^* u_{k_1} u_{k_2}^2 + \gamma_{k_2} u_{k_1} u_{k_2}^{*2}\big] \\ & + \sum_{k_1=1}^{2} \sum_{\substack{k_2=1 \\ k_2 \neq k_1}}^{2} \acute{h}_{k_1,k_1,k_2}^{(i)} \big[u_{k_1}^2 u_{k_2}^* + \gamma_{k_2}^* u_{k_1}^2 u_{k_2}\big] \end{aligned} \tag{6}$$

where

$$\begin{aligned} \acute{h}_k^{(i)} &= h_k^{(i)} \; a_k \zeta_k \\ \acute{h}_{k_1,k_2,k_2}^{(i)} &= h_{k_1,k_2,k_2}^{(i)} \; a_{k_1} \left|a_{k_2}\right|^2 \zeta_{k_1} \left|\zeta_{k_2}\right|^2 \\ \acute{h}_{k_1,k_1,k_2}^{(i)} &= h_{k_1,k_1,k_2}^{(i)} \; a_{k_1}^2 a_{k_1}^* \zeta_{k_1}^2 \zeta_{k_2}^*. \end{aligned} \tag{7}$$

It can be noted that the additional terms in (6) compared with (4) are scaled by γ. That is, the distortion levels resulting from static I/Q imbalanced sources exciting a nonlinear MIMO Volterra series are proportional to the levels of IRR.

III. Compensation of Joint Static I/Q Imbalance and Dynamic MIMO PA Distortion

Section II describes the joint effects of static I/Q imbalance sources exciting a nonlinear MIMO Volterra series in (6). It can be noted that the additional basis functions in (6) can be compensated by augmenting conjugate basis functions or by separating the I/Q components, as described in [20] and [21] for SISO transmitters. In this section, these mitigation techniques are transformed for MIMO transmitters for the joint mitigation of static I/Q imbalance and dynamic MIMO PA distortions.

A. MIMO Memory Polynomial

The MIMO memory polynomial (MP) model is presented in this section as a reference model based on [45] for the compensation of nonlinear distortions in an MIMO PA. In [32], the MIMO MP model presents a pruning of the MIMO Volterra model [33], [44] suitable for practical implementations. Therefore, the MIMO MP model can be described as [32]

$$y_i^{\mathrm{MP}}(n) = \sum_{\substack{p=1 \\ \text{p odd}}}^{P} \bar{H}_p^{(i)}[\{u_k\}_{k=1}^K] \tag{8}$$

where $\bar{H}_p^{(i)}$ denotes the pth order nonlinear MIMO MP operator for the ith output and can be described as

$$\begin{aligned} & \bar{H}_p^{(i)}\left[\{u_k\}_{k=1}^K\right] \\ & = \sum_{m=0}^{M_p} \sum_{k_1=1}^{K} \cdots \sum_{k_{\frac{p+1}{2}}=1}^{K} \sum_{\ell_1=1}^{K} \cdots \sum_{\ell_{\frac{p-1}{2}}=1}^{K} \\ & \quad h_{k_1,\ldots,k_{\frac{p+1}{2}},\ell_1,\ldots,\ell_{\frac{p-1}{2}}}^{(i)}(m) \prod_{q=1}^{\frac{p+1}{2}} u_{k_q}(n-m) \prod_{r=1}^{\frac{p-1}{2}} u_{\ell_r}^*(n-m) \end{aligned} \tag{9}$$

where P is the nonlinear order and M_p denotes the memory depth for the pth nonlinear order.

Considering a static MIMO MP model with $K = 2$, $p = 3$, and $M_p = 0$ in (9) and compared with (6), it can be noted that the additional terms introduced by I/Q imbalance impairments in (6) are not considered in the MIMO MP model. Therefore, the MIMO MP model compensates only the MIMO PA distortion but not the joint I/Q imbalance and MIMO PA distortion. Since it is widely used, the MIMO MP model is used as a baseline for comparison with the proposed models.

B. Augmented Complex Conjugate Model

From (1), it can be noted that I/Q imbalance distortions result in the addition of a conjugate replica to the complex-valued baseband input signal. Therefore, the augmented complex conjugate (ACC) model augments an additional branch of basis functions to the MIMO MP model. These augmented basis functions are complex conjugate pairs of the MIMO MP basis functions. This model is based on [21] bringing this SISO model to the MIMO scenario. The ACC model allows for greater scope to compensate the I/Q imbalance distortion terms described in (6). The ith output for the ACC model is then described as

$$y_i^{\mathrm{ACC}}(n) = \sum_{\substack{p=1 \\ \text{p odd}}}^{P} \bar{H}_p^{(i)}\left[\left\{u_k\right\}_{k=1}^K\right] + \sum_{\substack{p=1 \\ \text{p odd}}}^{P} \bar{H}_p^{(i)}\left[\left\{u_k^*\right\}_{k=1}^K\right] + c_i \tag{10}$$

where c_i denotes the local oscillator leakage dc offset compensator.

C. Augmented Linear Complex Conjugate Model

From the MIMO Volterra series as shown in Fig. 1, it can be noted that the linear and nonlinear distortions in an MIMO transmitter are additive. For hardware implementations where linear distortions are significant and of the same level as the nonlinear PA distortions, the ACC model can be simplified by adding a complex conjugate pair to the linear terms of the MIMO MP model, referred to as the augmented linear complex conjugate (ALCC) model. The ith output for the ALCC model is then described as

$$y_i^{\mathrm{ALCC}}(n) = \sum_{\substack{p=1 \\ \text{p odd}}}^{P} \bar{H}_p^{(i)}\left[\left\{u_k\right\}_{k=1}^K\right] + \bar{H}_1^{(i)}\left[\left\{u_k^*\right\}_{k=1}^K\right] + c_i. \tag{11}$$

TABLE I
SUMMARY OF THE PROPOSED MODELS FOR MITIGATING JOINT I/Q IMBALANCE AND MIMO PA DISTORTION

Acronym	Method	Eq.	Features
MP [32]	Pruned MIMO Volterra	(8), (9)	Mitigates only MIMO PA distortion Does not mitigate joint I/Q imbalance and MIMO PA distortion
ACC [21]	MIMO MP augmented with its complex conjugate pairs	(10)	Broadens the scope of MIMO MP Mitigates joint I/Q imbalance and MIMO PA distortion
ALCC	MIMO MP augmented with its linear complex conjugate pairs	(11)	Simplification of the ACC model Mitigates joint I/Q imbalance and linear MIMO PA distortion
RMP [20]	MP model applied to real and imaginary parts separately	(12)	Modeling approach for I/Q Imbalance mitigation I and Q branches treated as separate inputs Mitigates joint I/Q imbalance and MIMO PA distortion

D. Real-Valued MIMO MP Model

The real-valued MIMO MP (RMP) model is based on [20], which takes a modeling approach by considering the I/Q branches as separate input signals to compensate I/Q imbalance effects in SISO PAs. This paper brings the work done for SISO PAs in [20] to an MIMO framework by separating the real and imaginary parts of the input and applying the MIMO MP model on this real-valued data. For a $K \times K$ MIMO transmitter, the ith output for the RMP model in its complex-valued baseband form is

$$y_i^{\mathrm{RMP}}(n) = \sum_{\substack{p=1 \\ \text{p odd}}}^{P} \bar{H}_p^{(i)}\left[u_1^R, u_1^I, \ldots, u_K^R, u_K^I\right] \tag{12}$$

where u^R and u^I denote the respective real and imaginary parts of the complex-valued signals. A summary of the proposed techniques is given in Table I.

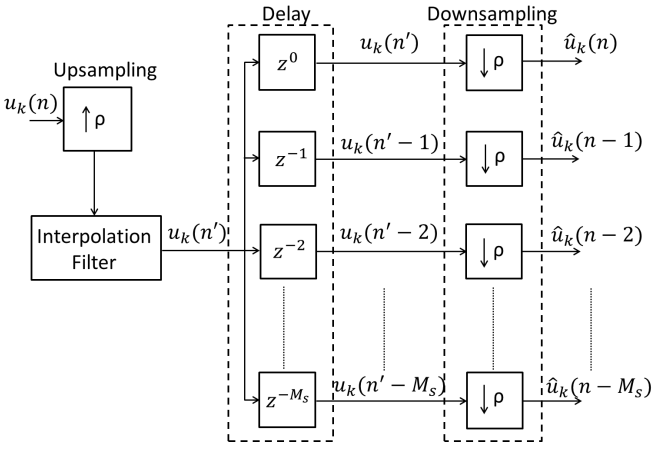

Fig. 2. Subsample FIR basis for mitigating dynamic I/Q imbalance distortions.

IV. COMPENSATION OF JOINT DYNAMIC I/Q IMBALANCE AND DYNAMIC MIMO PA DISTORTION

The model presented in (1) and (2) deals only with static I/Q imbalance distortions. However, as the signal bandwidth increases, the description of RF MIMO transmitter impairments requires the study of dynamic I/Q imbalance distortions as well. This paper combines a subsample (multirate) resolution technique with the models described in Section III to mitigate the joint dynamic I/Q impairments and nonlinear effects. Multirate processing has been used in the modeling and predistortion of nonlinear effects in PAs [46], [47]. Different multirate branches are used to improve the modeling and linearization ability of standard models in [46]. Furthermore, multirate processing is also used in expanding the digital bandwidth of signals to capture distortion effects that are otherwise not considered [47].

The proposed multirate method uses a set of finite impulse response (FIR) basis functions in subsample domain to combat dynamic I/Q imbalance effects. The amplitude and phase variations between the I/Q branches can be understood as FIR in subsample domain [24], [41], [42]. Furthermore, subsampled time misalignments between the I/Q branches occur during the digital to analog conversion process due to imperfect hardware synchronization. These effects are compounded in RF MIMO transmitters, where multiple I/Q signals can all be time misaligned with each other. Hence, FIR basis functions in subsample domain combat the dynamic I/Q impairments exhibited by the hardware.

In subsample resolution, the input signal is first upsampled by a factor ρ and delayed by M_s samples. These delayed versions are then downsampled by the same factor to generate a set of FIR basis functions in the same time scale. This process is shown in Fig. 2. Hence, the resulting subsample resolution FIR model can be described as

$$H_s^{(i)}\left[\hat{u}\right] = \sum_{m_s=0}^{M_s} h_s^{(i)}\left(m_s\right)\hat{u}\left(n - m_s\right) \tag{13}$$

where $\hat{u}$ denotes the output FIR basis with subsample resolution. $H_s^{(i)}[\hat{u}]$ and $h_s^{(i)}(m_s)$ denote the subsample FIR model operator and coefficients, respectively.

The proposed models for mitigating static I/Q imbalance distortions are enhanced for the compensation of dynamic I/Q imbalance with a subsample resolution of $1/\rho$ samples and a memory of M_s samples in the same time scale. The enhanced models can then be described as

$$\hat{y}_i^{\mathrm{ACC}}(n) = H_s^{(i)}\left[\hat{u}\right] + \sum_{\substack{p=1 \\ \text{p odd}}}^{P} \bar{H}_p^{(i)}\left[\{u_k\}_{k=1}^K\right] + \sum_{\substack{p=1 \\ \text{p odd}}}^{P} \bar{H}_p^{(i)}\left[\{u_k^*\}_{k=1}^K\right] + c_i$$

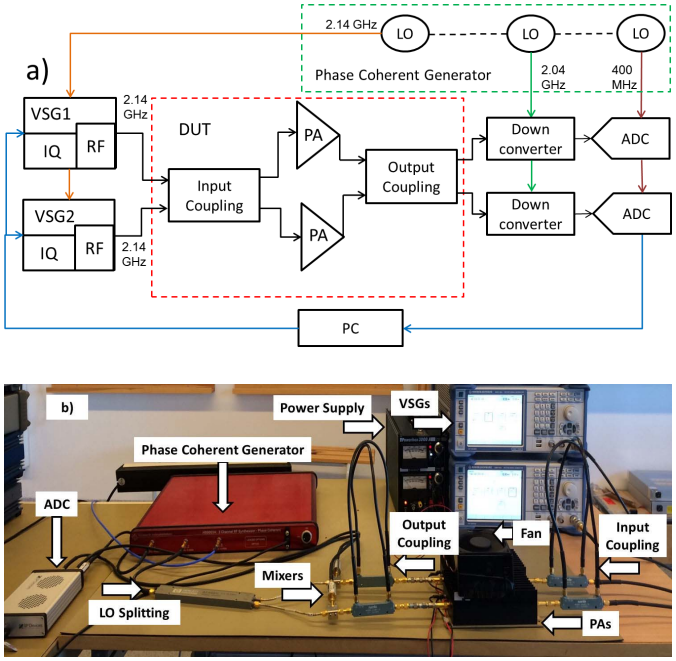

Fig. 3. (a) Outline of the measurement setup used in experiments depicting two independent I/Q imbalanced sources exciting an MIMO PA, the down conversion process and measurement with ADC. (b) Measurement setup used in experiments.

$$\hat{y}_i^{\mathrm{ALCC}}(n) = H_s^{(i)}\left[\hat{u}\right] + \sum_{\substack{p=1 \\ \text{p odd}}}^{P} \bar{H}_p^{(i)}\left[\{u_k\}_{k=1}^{K}\right] + \sum_{\substack{p=1 \\ \text{p odd}}}^{P} \bar{H}_1^{(i)}\left[\{u_k^*\}_{k=1}^{K}\right] + c_i$$

$$\hat{y}_i^{\mathrm{RMP}}(n) = H_s^{(i)}\left[\hat{u}\right] + \sum_{\substack{p=1 \\ \text{p odd}}}^{P} \bar{H}_p^{(i)}\left[u_1^R, u_1^I, \ldots, u_K^R, u_K^I\right] \quad (14)$$

where $\hat{y}_i^{\mathrm{ACC}}(n)$, $\hat{y}_i^{\mathrm{ALCC}}(n)$, and $\hat{y}_i^{\mathrm{RMP}}(n)$ are ith output signals for the enhanced ACC, ALCC, and RMP models. Since, the proposed models in (14) are linear in parameters, the corresponding coefficients can be determined using least squares estimation techniques. Furthermore, nonlinear dynamic I/Q imbalance distortions may also be considered. However, the compensation of these distortions would require high complexity nonlinear models in subsample resolution.

V. Experimental Investigation

A. Setup

Experiments are performed to analyze the error performance of the proposed models for a measurement setup mimicking a typical fourth generation (4G) 2×2 RF MIMO transmitter. An outline of the measurement setup used in the experiments is shown in Fig. 3(a), whereas the actual measurement setup is shown in Fig. 3(b). The device-under-test (DUT) is excited by two R&S SMBV100A vector signal generators (VSGs). The VSGs enhance RF phase coherency using an HS9003 signal generator from Holzworth Instrumentation [48].

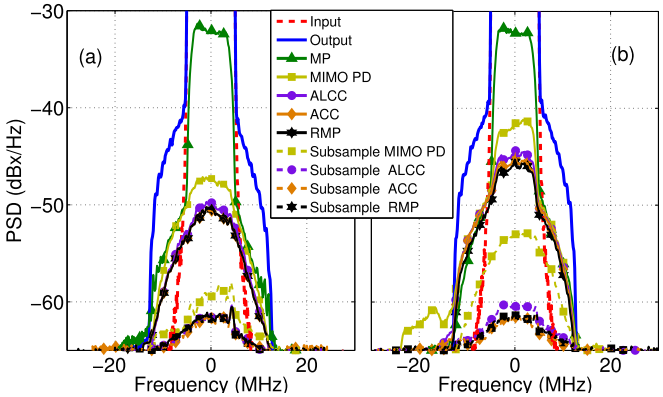

Fig. 4. DPD error spectrum of the proposed models with 10-MHz signals and crosstalk levels of (a) −30 and (b) −20 dB.

The HS9003 gives phase coherent RF outputs and is used as a common external local oscillator. The outputs from the DUT are measured using wideband down converters cascaded to a two-channel 14-b resolution analog-to-digital-converter (ADC) operating at a sampling frequency of 400 MHz. The ADCs and the VSGs are then connected through a PC for control.

The DUT consists of two ZVE-8G+ PAs placed between two coupling stages used for introducing crosstalk effects [31]–[33], [35]. The ZVE-8G+ PAs have a gain of 30 dB each and a 1-dB compression point of 30 dBm. The DUT is excited by two independently generated quadrature amplitude modulated signals with peak-to-average power ratio ≈7.5 dB and root mean square power level of −7 dBm. The signals are created in a PC with 4×10^5 complex-valued samples that are uploaded to the VSGs and upconverted to 2.14 GHz to excite the DUT.

DPD is performed for the proposed models using indirect learning architecture [11]. The amplitude imbalance is set with $\alpha_1 = 0.05$ and $\alpha_2 = -0.04$ with a phase imbalance $\theta_1 = 4°$ and $\theta_2 = -5°$ and a gain imbalance $\zeta_k = 0.9$. These parameter settings are in accordance with practical implementations [43]. The performance of the proposed models is also compared with the MIMO PD presented in [49].

B. Results

First, the measurements are performed for crosstalk at both the input and output ranging from −40 to −10 dB with 10-MHz signal bandwidth. The proposed models are set with nonlinear order, $P = 5$, and a pruned memory scheme, where $M_1 = 5$, $M_3 = 2$, and $M_5 = 0$. That is, the linear kernel memory depth is 5, the third-order kernel memory depth is 2, and the fifth order kernel is static. For subsample resolution, the appended linear FIR model is set with $M_s = 5$ and $\rho = 5$.

1) Crosstalk: The DPD error spectrum of the proposed models with respect to a normalized carrier is plotted for −30-dB crosstalk in Fig. 4(a) and for −20-dB crosstalk in Fig. 4(b). These results are summarized in Table II with respect to the normalized mean squared error (NMSE) and adjacent channel to power ratio (ACPR).

For −30-dB crosstalk, it can be noted that the error for the MIMO MP model is the highest with NMSE of −45.3 dB and

TABLE II

IN-BAND AND OUT OF BAND DPD ERROR PERFORMANCE AND COMPUTATIONAL COMPLEXITY OF THE PROPOSED MODELS FOR 10-MHz SIGNALS WITH CROSSTALK LEVELS OF −30 AND −20 dB

Method	w/o sub-sample resolution					with sub-sample resolution				
	NMSE (dB)		ACPR (dB)		FLOPs (#)	NMSE (dB)		ACPR (dB)		FLOPs (#)
	Crosstalk -30 (dB)	Crosstalk -20 (dB)	Crosstalk -30 (dB)	Crosstalk -20 (dB)		Crosstalk -30 (dB)	Crosstalk -20 (dB)	Crosstalk -30 (dB)	Crosstalk -20 (dB)	
no DPD	-16.1	-9.5	-27.5	-20.7	-	-16.1	-9.5	-27.5	-20.7	-
MP	-31.5	-30.9	-50.9	-51.0	414	-	-	-	-	-
MIMO PD [50]	-45.3	-40.6	-51.4	-50.9	252	-52.0	-48.5	-54.7	-52.5	406
ALCC	-47.6	-43.1	-52.3	-51.3	488	-54.1	-53.5	-57.5	-56.9	642
ACC	-48.0	-43.6	-52.4	-51.4	668	-54.2	-54.0	-57.5	-57.0	822
RMP	-48.2	-44.2	-52.6	-52.2	484	-54.3	-54.1	-57.8	-57.0	590

ACPR of −51.4 dB, whereas the RMP model achieves the lowest error among the proposed models with NMSE of −48.0 dB and ACPR of −52.4 dB. The ALCC and ACC models also achieve much lower levels of error performance compared with the MIMO MP model. The MIMO PD performs better than the MIMO MP model, since it considers I/Q imbalance but worse than any of the proposed models, since it only considers self-kernels for crosstalk and not the cross kernels.

For −20-dB crosstalk, it can be noted that the proposed models follow a similar trend, where MIMO MP model achieves worst error performance with NMSE of −30.9 dB and ACPR of −51.0 dB and the RMP model achieves lowest error with NMSE of −44.2 dB and ACPR of −52.2 dB. Furthermore, it can be noted that the error for each of the proposed models is marginally higher for −20-dB crosstalk than −30-dB crosstalk reflecting the degradation introduced by an increased crosstalk level between the transmission paths.

The compensation ability of the proposed models can be analyzed qualitatively by comparing the basis functions of the proposed models with the basis of the I/Q imbalanced sources exciting a nonlinear MIMO Volterra series (see Fig. 1). For this purpose, consider again the example of two independent I/Q imbalanced sources exciting a static third-order 2 × 2 MIMO PA, as described by (6) in Section II. The resulting basis functions are listed in Table III and compared with the basis of each of the proposed models. It can be noted that the MP model accounts for the fewest basis functions, since it does not consider any joint I/Q imbalance and MIMO PA distortion. The ACC model includes some of the additional terms by appending complex conjugate basis to the MP model. The RMP model takes a modeling approach toward mitigating the joint I/Q imbalance and MIMO PA distortion. It accounts for each of the basis functions listed in Table III by including all possible interactions between the real and imaginary parts of the I/Q imbalanced input signal. Hence, the error performance of the RMP method is better than the ACC and ALCC methods, as shown in the results (see Fig. 4 and Table II).

The error performance of each of the proposed models improves dramatically in subsample resolution, as depicted by the DPD error spectrum in Fig. 4, and the levels of NMSE and ACPR listed in Table II. It can be noted that the error

TABLE III

COMPARISON BETWEEN THE COMPENSATION ABILITY OF THE PROPOSED MODELS FOR A STATIC THIRD-ORDER 2 × 2 MIMO TRANSMITTER. COMPENSATED BASIS INDICATED BY ✓. UNCOMPENSATED BASIS INDICATED BY ×

Complex-valued models				Real valued model	
Basis functions to compensate	MP	ACC	ALCC	Basis functions to compensate	RMP
u_k	✓	✓	✓	u_k^R	✓
u_k^*	×	✓	✓	u_k^I	✓
$u_{k_1}\lvert u_{k_2}\rvert^2$	✓	✓	✓	$u_{k_1}^R u_{k_2}^R u_{k_3}^R$	✓
$u_{k_1}^*\lvert u_{k_2}\rvert^2$	×	✓	×	$u_{k_1}^R u_{k_2}^R u_{k_3}^I$	✓
$u_{k_1} u_{k_2}^{*2}$	×	×	×	$u_{k_1}^I u_{k_2}^I u_{k_3}^I$	✓
$u_{k_1} u_{k_2}^2$	×	×	×	$u_{k_1}^I u_{k_2}^I u_{k_3}^R$	✓
$u_{k_1}^2 u_{k_2}^*$	✓	✓	✓	-	-
$u_{k_1}^2 u_{k_2}$	×	×	×	-	-

observed in subsample resolution for the proposed models is close to the noise floor of the measurements, and the NMSE of the proposed models improves by a factor of 6 dB for −30-dB crosstalk and by a factor of 10 dB for −20-dB crosstalk. The proposed models achieve an NMSE of −54 dB for −30-dB crosstalk and an NMSE of −53 dB for −20-dB crosstalk. Furthermore, the error performance of the MIMO PD also improves with NMSE of −52.0 dB for −30-dB crosstalk and −48.5 dB for −20-dB crosstalk but it is still worse than the proposed models.

These results show the importance of mitigating dynamic I/Q imbalance distortions in RF MIMO transmitters, especially at higher crosstalk levels, which represents a key contribution of this paper. The subsampling method is presented only for linear dynamic I/Q imbalance distortions. A full description of such dynamics effects would require a large number of nonlinear basis functions in subsample resolution. However, the contribution of such terms is small compared with the terms considered in this paper, due to the crosstalk being less than 1.

The computational complexity of the proposed models is described in terms of the number of floating point

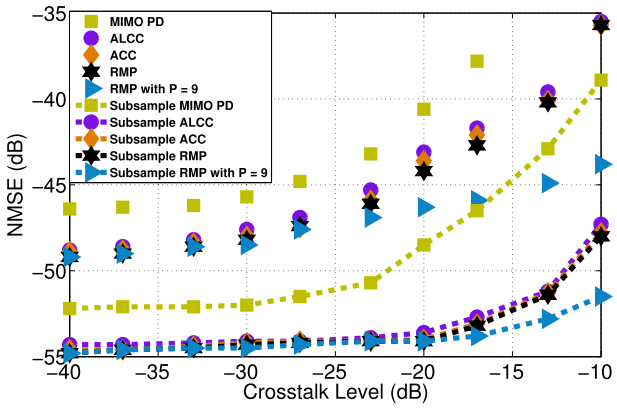

Fig. 5. DPD error performance in terms of NMSE of the proposed models for 10-MHz signals with crosstalk levels ranging from −40 to −10 dB.

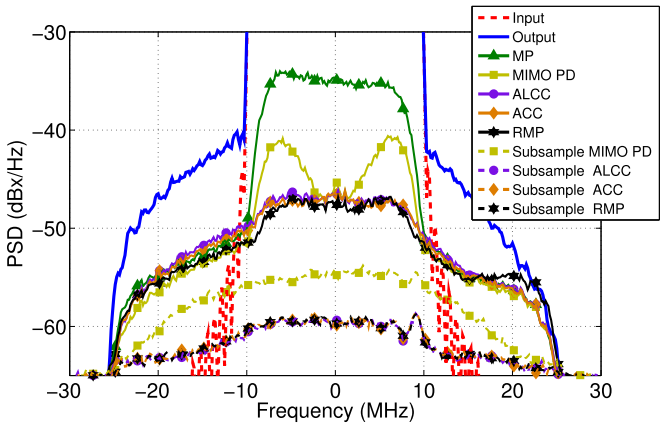

Fig. 6. DPD error spectrum of the proposed models for 20-MHz signals and −20-dB crosstalk.

operations (FLOPs) in Table II. A detailed analysis of the computational complexity of the proposed models is described in Section VI. It can be noted that the computational complexity of the MIMO PD is the lowest with 252 FLOPs, since it does not consider any cross kernels. Furthermore, the computational complexity of the RMP and ALCC models is the lowest amongst the proposed models with 484 and 488 FLOPs, respectively, while the ACC model requires the highest computational complexity with 668 FLOPs. The computational complexity of the proposed models in subsample resolution increases by 154 additional FLOPs for the MIMO PD, ALCC, and ACC models and 106 additional FLOPs for the RMP model. Therefore, the computational complexity increases significantly for the MIMO PD model by 60%. However, the complexity increases marginally by 35%, 23%, and 21% for the ALCC, ACC, and RMP models, respectively, whereas the NMSE improves by 10 dB for each of the proposed models.

Fig. 5 plots the NMSE of the proposed models over different levels of crosstalk ranging from −40 to −10 dB. It can be noted that the NMSE degrades with increasing crosstalk levels for all the proposed models without subsampling. It can be noted that the performance degrades when the crosstalk increases from −30 to −20 dB, where the NMSE for the proposed models falls from −49 to −44 dB. The degradation is particularly severe as the crosstalk increases from −20 to −10 dB, where the NMSE of the proposed models falls to −35 dB. It can be noted that increased crosstalk levels result in stronger nonlinear distortions, which can be compensated with higher model orders. This is shown in Fig. 5, where the RMP model with $P = 9$ achieves NMSE of −43.8 dB. Furthermore, the corresponding NMSE of the proposed models achieved with subsample resolution is also plotted in Fig. 5. It can be noted that the additional joint I/Q imbalance and MIMO PA distortions introduced by increasing crosstalk levels are mitigated with subsample resolution gain by a factor of upto 10 dB. Thus, each of the proposed models achieve −54-dB NMSE with subsample resolution for crosstalk levels upto −20 dB and NMSE of −48 dB for crosstalk levels upto −10 dB. However, the RMP model in subsample resolution with $P = 9$ achieves NMSE of −51.5 dB for crosstalk levels of −10 dB.

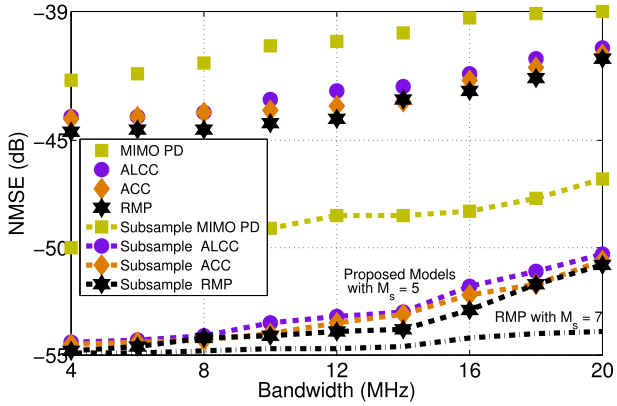

Fig. 7. DPD error performance in terms of NMSE of the proposed models for signals with bandwidth ranging from 4 to 20 MHz and −20-dB crosstalk.

This paper also investigates the effect of increasing bandwidth on the performance of the proposed models. Therefore, the DPD error spectra of the proposed models for 20 MHz signals are depicted in Fig. 6.

2) Bandwidth: Fig. 7 plots DPD error performance of the proposed models with and without subsample resolution in terms of NMSE over signals of bandwidth ranging from 4 to 20 MHz based on 4G LTE communication standards [50]. It can be noted that the error performance of the proposed models suffers with increasing bandwidth without subsampling due to greater impact of dynamic I/Q imbalance distortions. Therefore, subsample resolution FIR basis functions play a more important role in compensating these dynamic I/Q imbalance distortions resulting in NMSE of −50 dB for all the proposed models, as shown in Fig. 7. Furthermore, it can be noted that even with subsample resolution, the performance degrades by 3 dB as the bandwidth increases from 10 to 20 MHz. However, this degradation can be compensated with a higher complexity model, as shown in Fig. 7 for the RMP model with $M_s = 7$.

Since carrier aggregated channels typically require higher bandwidth signals [50], the error performance is analyzed for signal bandwidth upto 65 MHz in Table IV. The RMP model

TABLE IV
ERROR PERFORMANCE OF THE RMP MODEL WITH VARYING COMPLEXITY FOR HIGHER BANDWIDTH SIGNALS WITH −20- dB CROSSTALK

$P, M_1, \cdots, M_P, M_s$	NMSE (dB)					FLOPs (#)
	5 MHz	20 MHz	35 MHz	50 MHz	65 MHz	
no DPD	-12.7	-9.2	-6.8	-2.7	-1.5	-
5, 5, 2, 0, 5	-54.7	-50.8	-46.5	-41.2	-32.1	590
5, 7, 2, 0, 7	-54.5	-53.9	-49.2	-47.3	-41.2	662
5, 7, 3, 1, 9	-49.1	-52.9	-51.1	-49.4	-43.4	1042
5, 7, 4, 2, 1, 9	-42.1	-48.2	-49.4	-51.5	-48.2	2034

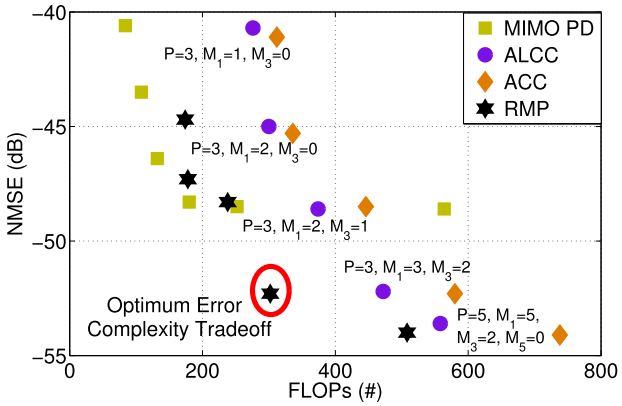

Fig. 8. Comparison between the NMSE versus the computational complexity of the proposed models for 10-MHz signals and −20-dB crosstalk. The proposed models are compared for different nonlinear orders and memory.

with subsample resolution is used with different complexities. It can be noted that higher bandwidth signals require higher complexity models to achieve NMSE of ∼−50 dB. For 65-MHz signals, the subsample RMP model achieves −48.2-dB NMSE but requires 2034 FLOPs, which is 4 times higher than the FLOPs required for compensating 20-MHz signals. It can also be noted that the NMSE performance for lower bandwidth signals degrades with increasing complexity due to overmodeling. For instance, the 5-MHz signal achieves −54.7-dB NMSE with 590 FLOPs but its performance degrades to −42.1-dB NMSE for an RMP model that requires 2034 FLOPs.

3) Complexity and Error Performance: Finally, Fig. 8 plots the NMSE of the proposed models versus their computational complexity for different combinations of nonlinear order and memory. The signal bandwidth is 10 MHz and the crosstalk level is −20 dB. It can be noted that the MIMO PD achieves the worst NMSE performance even at higher computational complexity. The ACC and ALCC models achieve lower error at the expense of higher computational complexity. However, the RMP model achieves the best balance among the models presented in this paper between error performance and complexity for this scenario.

Based on the experimental results provided in this section, it can be concluded that the RMP model appended with linear FIR basis in subsample resolution provides the best balance amongst the proposed models between error performance and computational complexity for mitigating joint I/Q imbalance and dynamic MIMO PA distortion for a 2×2 MIMO transmitter.

VI. COMPLEXITY ANALYSIS OF THE PROPOSED MODELS

In this section, the performance of the proposed models described in Section V-B is analyzed with respect to their computational complexity. With an increase in the number of carriers in MIMO transmitters, computational complexity plays an important role when implementing compensation techniques in digital platforms. Hence, the complexity of the proposed models is compared based on the number of FLOPs needed to implement them.

Following the methodology in [51], the computational complexity of the proposed models is evaluated as the sum of the total number of FLOPs required in: 1) creation of the basis functions and 2) multiplication of the basis functions with their respective model coefficients referred to as the filtering process.

A. Complexity of MIMO MP

The filtering process for the MIMO MP model involves multiplication of the complex-valued coefficients $h^{(i)}_{k_1,\ldots,k_{p+1/2},k_1,\ldots,\ell_{p-1/2}}(m)$ with their respective basis functions. Therefore, the filtering complexity of the MIMO MP model depends on the total number of basis functions.

From (9), it can be noted that the total number of linear basis functions in the MIMO MP model is $K(M+1)$, whereas the total number of the pth nonlinear order basis functions, $N^{\mathrm{MP}}_{b_p}$, is given as

$$N^{\mathrm{MP}}_{b_p} = \begin{pmatrix} K + \dfrac{p+1}{2} - 1 \\ \dfrac{p+1}{2} \end{pmatrix} \begin{pmatrix} K + \dfrac{p+1}{2} - 2 \\ \dfrac{p+1}{2} - 1 \end{pmatrix}. \quad (15)$$

Then, the filtering complexity of the MIMO MP model, C^{MP}_f, can be written in terms of the number of FLOPS as

$$C^{\mathrm{MP}}_f = 6\left[K(M_1+1) + \sum_{\substack{p=3 \\ \text{p odd}}}^{P} N^{\mathrm{MP}}_{b_p}(M_p+1)\right]. \quad (16)$$

Next, the computational complexity of creating the basis functions for the MIMO MP model is evaluated. From (9), it can be noted that the basis functions for the MIMO MP model require $p-1$ complex-valued multiplications to compute the product $\prod_{q=1}^{p+1/2} u_{k_q}(n-m)\prod_{r=1}^{p-1/2} u^*_{\ell_r}(n-m)$. However, this complexity can be reduced by noticing the combinations of terms of the form $u_{k_q}(n-m)$

TABLE V
NUMBER OF TERMS N_g^p BELONGING TO THE COMPLEXITY REDUCED GROUP $\Omega_g(p)$ FOR A 2×2 MIMO PA

p \ g	1	2	3	4	5	$\sum_g N_g^p$
3	4	-	-	-	-	4
5	5	6	-	-	-	11
7	4	9	6	-	-	19
9	4	6	8	10	-	28
11	4	6	9	9	12	40

$\left|u_{k_q}(n-m)\right|^2$ when $j_q = \ell_r$ in (9). Consider the example of the third-order static nonlinear terms in (9) for a 2×2 MIMO PA

$$\begin{aligned} H_3^{(i)}&\left[\{u_k\}_{k=1}^2\right] \\ &= \left[h_{111}^{(i)} u_1(n)\,|u_1(n)|^2 + h_{122}^{(i)} u_1(n)\,|u_2(n)|^2 \right. \\ &\quad + h_{211}^{(i)} u_2(n)\,|u_1(n)|^2 + h_{222}^{(i)} u_2(n)\,|u_2(n)|^2 \left.\right] \\ &\quad + \left[h_{112}^{(i)} u_1^2(n) u_2^*(n) + h_{221}^{(i)} u_2^2(n) u_1^*(n)\right]. \end{aligned} \tag{17}$$

From (17), it can be noted that there are four terms of the form $u_k\,|u_\ell|^2$, which have a computational complexity of five FLOPs each while there are two terms of the form $u_k^2 u_\ell^*$, which have a computational complexity of 18 FLOPs each. Therefore, basis functions of the MIMO MP model can be classified into groups of different complexities. Hence, the computational complexity of creating basis functions for the MIMO MP model can be described in terms of the computational complexity of each of these groups and the number of basis functions belonging to each group.

In general, the possible groups $\Omega_g(p)$ that contain terms of the form $u\,|u|^{2g}$ for a pth order nonlinearity can be described as

$$\Omega_g(p) = \prod_{q=1}^{\frac{p+1}{2}-g} u_{k_q}(n-m)\left|u_{k_q}^*(n-m)\right|^g \prod_{r=1}^{\frac{p-1}{2}-g} u_{\ell_r}^*(n-m). \tag{18}$$

The corresponding number of terms N_g^p in the group $\Omega_g(p)$ for different nonlinear orders p is given for a 2×2 MIMO PA in Table V. The resulting complexity $C(\Omega_g(p))$ of the group $\Omega_g(p)$ is given as

$$C(\Omega_g(p)) = 6(p-2g-1) + (g-1) + 2. \tag{19}$$

Finally, the computational complexity of creating the basis functions for the MIMO MP model, C_b^{MP}, can be described as

$$\begin{aligned} C_b^{\mathrm{MP}} &= \sum_{p=3}^{P} (M+1)\left(S_p + \bar{S}_p + 6\right) \\ S_p &= \sum_{g=1}^{\frac{p-1}{2}} N_g^p\, C\left(\Omega_g(p)\right) \\ \bar{S}_p &= 6\left(N_{bp}^{\mathrm{MP}} - \sum_{g=1}^{\frac{p-1}{2}} N_g^p\right)(p-1) \end{aligned} \tag{20}$$

where S_p denotes the total complexity of the terms of the form $u\,|u|^g$, while $\bar{S}_p$ denotes the complexity of the remaining terms.

B. Complexity of ACC

The complexity of creating basis functions for the ACC model is the same as the MIMO MP model, since the ACC basis functions do not require any additional FLOPs [51]. Thus, the complexity of creating basis functions for ACC model is $C_b^{\mathrm{ACC}} = C_b^{\mathrm{MP}}$.

However, the filtering complexity of the ACC model is double than the MIMO MP model, since it involves twice the number of basis functions. Hence, the filtering complexity of the ACC model, C_f^{ACC}, can be described as

$$C_f^{\mathrm{ACC}} = 6\left[2\left(K(M_1+1) + \sum_{\substack{p=3 \\ \text{p odd}}}^{P} N_{b_p}^{\mathrm{MP}}\left(M_p+1\right)\right)\right]. \tag{21}$$

C. Complexity of ALCC

The complexity of creating basis functions for the ALCC model is also the same as the MIMO MP model, since the ALCC basis do not require any additional FLOPs. Therefore, the basis creation complexity of the ALCC model is $C_b^{\mathrm{ALCC}} = C_b^{\mathrm{MP}}$. However, its filtering complexity increases due to the additional $M+1$ linear basis functions. Hence, the filtering complexity of the ALCC model, C_f^{ALCC}, can be described as

$$C_f^{\mathrm{ALCC}} = 6\left[2\left(K(M_1+1)\right) + \sum_{\substack{p=3 \\ \text{p odd}}}^{P} N_{b_p}^{\mathrm{MP}}(M_p+1)\right]. \tag{22}$$

D. Complexity of RMP

The filtering complexity of the RMP model is equal to the number of its basis functions, since it involves real-valued multiplications only. However, the number of basis functions itself is larger than the MIMO MP model. This is a result of separating the real and imaginary parts of the complex-valued baseband signals $\{u_k\}_{k=1}^K$, which increases the number of carriers to $2K$. These carriers are then combined without repetition to create the basis functions. Hence, the filtering complexity of the RMP model, C_f^{RMP}, can be described as

$$\begin{aligned} C_f^{\mathrm{RMP}} &= 6\left[2K(M_1+1) + \sum_{\substack{p=3 \\ \text{p odd}}}^{P} N_{b_p}^{\mathrm{MP}}(M_p+1)\right] \\ N_{b_p}^{\mathrm{MP}} &= \binom{2K+p-1}{p} \end{aligned} \tag{23}$$

where $N_{b_p}^{\mathrm{MP}}$ is the number of the pth order nonlinear basis functions for the RMP model.

The creation of each of the basis functions for the RMP model involves $p-1$ real-valued multiplications of the real and imaginary parts of the complex-valued baseband input signals. Hence, the complexity of creating basis functions for the RMP model, C_b^{RMP}, can be described as

$$C_b^{\mathrm{RMP}} = \sum_{\substack{p=3 \\ \text{p odd}}}^{P} N_{b_p}^{\mathrm{RMP}}(p-1)\left(M_p+1\right). \tag{24}$$

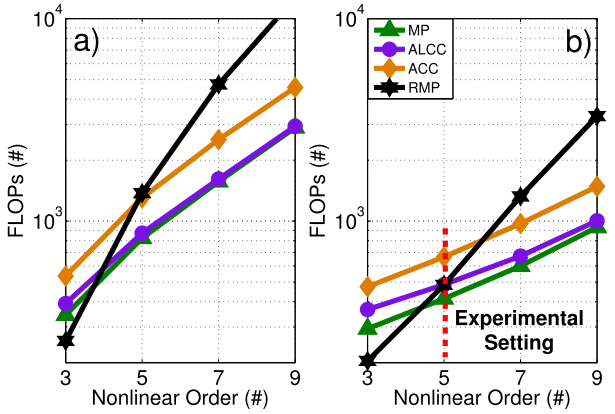

Fig. 9. Comparison between the computational complexity of the proposed models over different nonlinear orders. The proposed models are compared for (a) equal memory scheme and (b) pruned memory scheme.

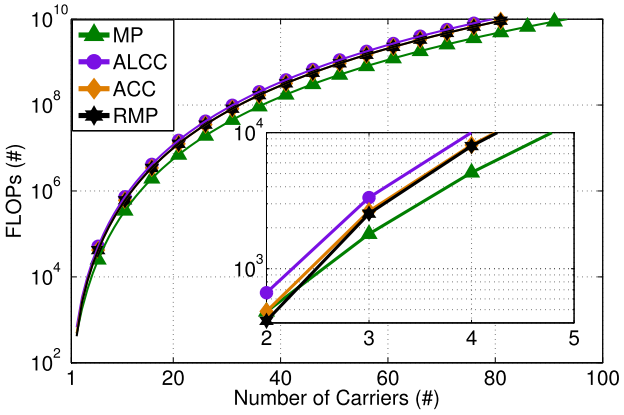

Fig. 10. Computational complexity of the proposed models over different number of carrier signals for $P = 5$ and a pruned memory scheme with $M_1 = 5$, $M_3 = 2$, and $M_5 = 0$.

E. Complexity of Subsampling

The oversampling method upsamples the input sequence and applies a low-pass interpolation filter to the expanded sequence. The interpolation filter is stored as a lookup-table, which adds a filtering complexity for the interpolation. The length of the real-valued interpolation filter is $N_{\text{interp}} \times \rho + 1$, where N_{interp} is the number of sample values used for interpolation. In this paper, $N_{\text{interp}} = 8$ and $\rho = 5$, since ideally $N_{\text{interp}} \leq 20$ and $\rho \leq 10$ [52]. Therefore, the interpolation filter consists of 41 real-valued coefficients, which require an additional 82 FLOPs to filter the upsampled sequence. The resulting interpolated sequence is then used to create the subsample resolution basis function with the delay operator, which requires no FLOPs [51]. Hence, the oversampling process only adds a filtering complexity for interpolation to all the proposed models.

Furthermore, filtering of the subsample resolution basis functions increases the complexity of the ACC and ALCC models by an additional $6K(M_s + 1)$ FLOPs, whereas, the complexity of the RMP model increases by an additional $2K(M_s + 1)$ FLOPs. For $K = 2$ and $M_s = 5$, the complexity increases by 72 FLOPs for the ACC and ALCC models and by 24 FLOPs for the RMP model.

Therefore, the subsampling method results in an additional 154 FLOPs for the ACC and ALCC models and 106 FLOPs for the RMP model.

F. Analysis

The computational complexity of the proposed models for different nonlinear orders is shown in Fig. 9(a) for an equal memory scheme, where $M_1 = M_3 = \cdots M_9 = 3$. It can be noted that the MIMO MP model achieves lowest computational complexity, because it does not add any additional basis to compensate for the I/Q imbalance distortions. The RMP requires the lowest complexity among the proposed models, since it uses real-valued multiplications. However, at higher nonlinear orders, the large number of basis functions involved in the RMP model begins to dominate its computational complexity. The complexity of the proposed models for a pruned memory scheme, where $M_1 = 5$, $M_3 = 2$, $M_5 = 0$, $M_7 = 0$, and $M_9 = 0$, is shown in Fig. 9(b). Similar trends are observed as Fig. 9(a), because the complexity of the proposed models increases linearly with memory and exponentially with nonlinear order.

The experiments in Section V are performed with $P = 5$ and the pruned memory scheme, as described in Fig. 9(b). Therefore, the MIMO MP model requires the lowest computational complexity, whereas the ACC model incurs the highest computational complexity. The complexity of the RMP model is comparable with the MIMO MP model, because the nonlinear order is low. These results are highlighted in Fig. 9(b).

The complexity of the proposed models with subsample resolution increases marginally due to the additional FLOPs required in the oversampling process and filtering the subsampled basis functions. However, a large gain in compensation ability can be achieved at the cost of marginal increase in complexity. This is shown in Table II for $K = 2$ and $M_s = 5$, where the error performance increases by 10 dB while the complexity increases marginally by 35%, 23%, and 21% for the ALCC, ACC, and RMP models, respectively.

Finally, the computational complexity of the proposed models is analyzed with respect to the number of carrier signals for deployment in the future higher order MIMO transmitters. Fig. 10 shows the complexity of the proposed models over different number of carrier signals for $P = 5$ and a pruned memory scheme with $M_1 = 5$, $M_3 = 2$, and $M_5 = 0$. It can be noted that the hardware effects change with the addition of more signals. Therefore, the model should consider only the dominant effects [53], i.e., the crosstalk is expected to reduce as the path is farther away. Another approach can be to transition toward a nonparametric description of the joint I/Q imbalance and MIMO PA distortion, which can be helpful in reducing the computational complexity [54].

VII. Conclusion

This paper proposes candidate solutions for the joint mitigation of I/Q imbalance and MIMO PA distortion with the aim to move toward a more complete description of hardware impairments for low cost RF MIMO transmitters. Therefore, candidate models for mitigating static I/Q imbalance distortions are proposed. The ACC model augments complex conjugate basis to the MIMO MP model, whereas the ALCC

model only augments conjugate terms to the linear basis of the MIMO MP model. The RMP model takes a modeling approach by treating the imbalanced I/Q branches as separate inputs to the MIMO MP model. The proposed models are linear in parameters and can be identified using least squares estimation techniques.

Furthermore, the proposed models are enhanced with linear subsample resolution to mitigate dynamic I/Q imbalance distortions resulting from time misalignments between the I/Q branches of the same (or different) signal sources. The proposed models achieve 10-dB gain in error performance even at a high crosstalk level of -10 dB and signal bandwidths ranging to 20 MHz with marginal increase in complexity with the subsampling method. Higher bandwidth signals for carrier aggregated LTE channels upto 65 MHz achieve ~ -50-dB NMSE but require high complexity models. This paper does not consider nonlinear subsample basis, since their contribution is small due to the crosstalk being less than 1.

Finally, the error performance and complexity of the proposed models are analyzed with measurements. It is noted that the ACC and ALCC models achieve similar error performance but suffer from high complexity. The RMP model achieves both the lowest error and the lowest complexity due to its ability to combat I/Q dynamic effects. However, with an increase in the number of carrier signals for MIMO, it is proposed that the models should consider only the adjacent crosstalk paths or transition toward a nonparametric description to alleviate their computational complexity.

REFERENCES

[1] G. J. Foschini and M. J. Gans, "On limits of wireless communications in a fading environment when using multiple antennas," *Wireless Pers. Commun.*, vol. 6, no. 3, pp. 311–335, Mar. 1998.

[2] G. C. Raleigh and J. M. Cioffi, "Spatio-temporal coding for wireless communication," *IEEE Trans. Commun.*, vol. 46, no. 3, pp. 357–366, Mar. 1998.

[3] V. K. V. Gottumukkala and H. Minn, "Capacity analysis and pilot-data power allocation for MIMO-OFDM with transmitter and receiver IQ imbalances and residual carrier frequency offset," *IEEE Trans. Veh. Technol.*, vol. 61, no. 2, pp. 553–565, Feb. 2012.

[4] G. Fettweis, M. Löhning, D. Petrovic, M. Windisch, P. Zillmann, and W. Rave, "Dirty RF: A new paradigm," *Int. J. Wireless Inf. Netw.*, vol. 14, no. 2, pp. 133–148, Jun. 2007.

[5] M. Faulkner and T. Mattsson, "Spectral sensitivity of power amplifiers to quadrature modulator misalignment," *IEEE Trans. Veh. Technol.*, vol. 41, no. 4, pp. 516–525, Nov. 1992.

[6] C.-L. Liu, "Impacts of I/Q imbalance on QPSK-OFDM-QAM detection," *IEEE Trans. Consum. Electron.*, vol. 44, no. 3, pp. 984–989, Aug. 1998.

[7] J. Tubbax *et al.*, "Compensation of IQ imbalance and phase noise in OFDM systems," *IEEE Trans. Wireless Commun.*, vol. 4, no. 3, pp. 872–877, May 2005.

[8] M. Isaksson, D. Wisell, and D. Rönnow, "A comparative analysis of behavioral models for RF power amplifiers," *IEEE Trans. Microw. Theory Techn.*, vol. 54, no. 1, pp. 348–359, Jan. 2006.

[9] M. Schetzen, "Theory of pth-order inverses of nonlinear systems," *IEEE Trans. Circuits Syst.*, vol. CAS-23, no. 5, pp. 285–291, May 1976.

[10] J. K. Cavers, "Amplifier linearization using a digital predistorter with fast adaptation and low memory requirements," *IEEE Trans. Veh. Technol.*, vol. 39, no. 4, pp. 374–382, Nov. 1990.

[11] C. Eun and E. J. Powers, "A new Volterra predistorter based on the indirect learning architecture," *IEEE Trans. Signal Process.*, vol. 45, no. 1, pp. 223–227, Jan. 1997.

[12] J. K. Cavers, "The effect of quadrature modulator and demodulator errors on adaptive digital predistorters for amplifier linearization," *IEEE Trans. Veh. Technol.*, vol. 46, no. 2, pp. 456–466, May 1997.

[13] J. K. Cavers, "New methods for adaptation of quadrature modulators and demodulators in amplifier linearization circuits," *IEEE Trans. Veh. Technol.*, vol. 46, no. 3, pp. 707–716, Aug. 1997.

[14] L. Ding, Z. Ma, D. R. Morgan, M. Zierdt, and G. T. Zhou, "Compensation of frequency-dependent gain/phase imbalance in predistortion linearization systems," *IEEE Trans. Circuits Syst. I, Reg. Papers*, vol. 55, no. 1, pp. 390–397, Feb. 2008.

[15] L. Anttila, M. Valkama, and M. Renfors, "Circularity-based I/Q imbalance compensation in wideband direct-conversion receivers," *IEEE Trans. Veh. Technol.*, vol. 57, no. 4, pp. 2099–2113, Jul. 2008.

[16] S. Boumaiza, J. Li, M. Jaidane-Saidane, and F. M. Ghannouchi, "Adaptive digital/RF predistortion using a nonuniform LUT indexing function with built-in dependence on the amplifier nonlinearity," *IEEE Trans. Microw. Theory Techn.*, vol. 52, no. 12, pp. 2670–2677, Dec. 2004.

[17] Y. D. Kim, E. R. Jeong, and Y. H. Lee, "Adaptive compensation for power amplifier nonlinearity in the presence of quadrature modulation/demodulation errors," *IEEE Trans. Signal Process.*, vol. 55, no. 9, pp. 4717–4721, Sep. 2007.

[18] H. Zareian and V. T. Vakili, "Analytical EVM, BER, and TD performances of the OFDM systems in the presence of jointly nonlinear distortion and IQ imbalance," *Ann. Telecommun.*, vol. 64, nos. 11–12, pp. 753–762, 2009.

[19] M. Aziz, M. Rawat, and F. M. Ghannouchi, "Rational function based model for the joint mitigation of I/Q imbalance and PA nonlinearity," *IEEE Microw. Wireless Compon. Lett.*, vol. 23, no. 4, pp. 196–198, Apr. 2013.

[20] H. Cao, A. S. Tehrani, C. Fager, T. Eriksson, and H. Zirath, "I/Q imbalance compensation using a nonlinear modeling approach," *IEEE Trans. Microw. Theory Techn.*, vol. 57, no. 3, pp. 513–518, Mar. 2009.

[21] L. Anttila, P. Händel, and M. Valkama, "Joint mitigation of power amplifier and I/Q modulator impairments in broadband direct-conversion transmitters," *IEEE Trans. Microw. Theory Techn.*, vol. 58, no. 4, pp. 730–739, Apr. 2010.

[22] L. Anttila, P. Händel, O. Mylläri, and M. Valkama, "Recursive learning-based joint digital predistorter for power amplifier and I/Q modulator impairments," *Int. J. Microw. Wireless Technol.*, vol. 2, no. 2, pp. 173–182, Apr. 2010.

[23] P. Zhan, K. Qin, and S. Cai, "Joint compensation model for memory power amplifier and frequency-dependent nonlinear IQ impairments," *Electron. Lett.*, vol. 47, no. 25, pp. 1382–1384, Dec. 2011.

[24] Z. Zhu, X. Huang, and H. Leung, "Joint I/Q mismatch and distortion compensation in direct conversion transmitters," *IEEE Trans. Wireless Commun.*, vol. 12, no. 6, pp. 2941–2951, Jun. 2013.

[25] M. Kim, Y. Maruichi, and J. I. Takada, "Parametric method of frequency-dependent I/Q imbalance compensation for wideband quadrature modulator," *IEEE Trans. Microw. Theory Techn.*, vol. 61, no. 1, pp. 270–280, Jan. 2013.

[26] W. Li, Y. Zhang, L.-K. Huang, J. Cosmas, C. Maple, and J. Xiong, "Self-IQ-demodulation based compensation scheme of frequency-dependent IQ imbalance for wideband direct-conversion transmitters," *IEEE Trans. Broadcast.*, vol. 61, no. 4, pp. 666–673, Dec. 2015.

[27] Y. Palaskas *et al.*, "A 5-GHz 108-Mb/s 2×2 MIMO transceiver RFIC with fully integrated 20.5-dBm P_{1dB} power amplifiers in 90-nm CMOS," *IEEE J. Solid-State Circuits*, vol. 41, no. 12, pp. 2746–2756, Dec. 2006.

[28] W.-C. Hua *et al.*, "Coupling effects of dual SiGe power amplifiers for 802.11n MIMO applications," in *Proc. IEEE Radio Freq. Integr. Circuits (RFIC) Symp.*, Jun. 2006, pp. 4–7.

[29] F. F. Dai, Y. Shi, J. Yan, and X. Hu, "MIMO RFIC transceiver designs for WLAN applications," in *Proc. 7th Int. ASIC Conf.*, Oct. 2007, pp. 348–351.

[30] T. Sadeghpour, R. A. Alhameed, N. T. Ali, I. T. E. Elfergani, Y. Dama, and O. O. Anoh, "Linear and nonlinear crosstalk in MIMO OFDM transceivers," in *Proc. 18th IEEE Int. Conf. Electron., Circuits, Syst. (ICECS)*, Dec. 2011, pp. 504–507.

[31] D. Saffar, N. Boulejfen, F. M. Ghannouchi, A. Gharsallah, and M. Helaoui, "Behavioral modeling of MIMO nonlinear systems with multivariable polynomials," *IEEE Trans. Microw. Theory Techn.*, vol. 59, no. 11, pp. 2994–3003, Nov. 2011.

[32] S. A. Bassam, M. Helaoui, and F. M. Ghannouchi, "Crossover digital predistorter for the compensation of crosstalk and nonlinearity in MIMO transmitters," *IEEE Trans. Microw. Theory Techn.*, vol. 57, no. 5, pp. 1119–1128, May 2009.

[33] S. Amin, P. N. Landin, P. Händel, and D. Rönnow, "Behavioral modeling and linearization of crosstalk and memory effects in RF MIMO transmitters," *IEEE Trans. Microw. Theory Techn.*, vol. 62, no. 4, pp. 810–823, Apr. 2014.

[34] E. Zenteno, R. Piazza, B. S. M. R. Rao, D. Rönnow, and B. Ottersten, "Low complexity predistortion and equalization in nonlinear multicarrier satellite communications," *EURASIP J. Adv. Signal Process.*, vol. 2015, no. 1, p. 30, 2015.
[35] P. M. Suryasarman and A. Springer, "A comparative analysis of adaptive digital predistortion algorithms for multiple antenna transmitters," *IEEE Trans. Circuits Syst. I, Reg. Papers*, vol. 62, no. 5, pp. 1412–1420, May 2015.
[36] P. Rabiei, W. Namgoong, and N. Al-Dhahir, "Reduced-complexity joint baseband compensation of phase noise and I/Q imbalance for MIMO-OFDM systems," *IEEE Trans. Wireless Commun.*, vol. 9, no. 11, pp. 3450–3460, Nov. 2010.
[37] D. Tandur and M. Moonen, "MIMO OFDM systems with digital RF impairment compensation," *Signal Process.*, vol. 90, no. 11, pp. 2965–2980, 2010.
[38] M. Marey, M. Samir, and M. H. Ahmed, "Joint estimation of transmitter and receiver IQ imbalance with ML detection for Alamouti OFDM systems," *IEEE Trans. Veh. Technol.*, vol. 62, no. 6, pp. 2847–2853, Jul. 2013.
[39] R. Rodriguez-Avila, G. Nunez-Vega, R. Parra-Michel, and A. Mendez-Vazquez, "Frequency-selective joint Tx/Rx I/Q imbalance estimation using Golay complementary sequences," *IEEE Trans. Wireless Commun.*, vol. 12, no. 5, pp. 2171–2179, May 2013.
[40] Ö. Özdemir, R. Hamila, and N. Al-Dhahir, "I/Q imbalance in multiple beamforming OFDM transceivers: SINR analysis and digital baseband compensation," *IEEE Trans. Commun.*, vol. 61, no. 5, pp. 1914–1925, May 2013.
[41] L. Anttila, M. Valkama, and M. Renfors, "Frequency-selective I/Q mismatch calibration of wideband direct-conversion transmitters," *IEEE Trans. Circuits Syst. II, Exp. Briefs*, vol. 55, no. 4, pp. 359–363, Apr. 2008.
[42] K. S. Lorenz, J. Goodman, G. Stantchev, and N. A. Pendergrass, "Generalized transmitter compensation of frequency dependent I/Q imbalance," *IEEE Trans. Signal Process.*, vol. 64, no. 9, pp. 2220–2231, May 2016.
[43] M. Inamori, A. M. Bostamam, Y. Sanada, and H. Minami, "IQ imbalance compensation scheme in the presence of frequency offset and dynamic DC offset for a direct conversion receiver," *IEEE Trans. Wireless Commun.*, vol. 8, no. 5, pp. 2214–2220, May 2009.
[44] A. K. Swain and S. A. Billings, "Generalized frequency response function matrix for MIMO non-linear systems," *Int. J. Control*, vol. 74, no. 8, pp. 829–844, 2001.
[45] M. Isaksson and D. Wisell, "Extension of the Hammerstein model for power amplifier applications," in *Proc. 63rd ARFTG Conf.*, Jun. 2004, pp. 131–137.
[46] D. D. Silveira, P. L. Gilabert, A. B. dos Santos, and M. Gadringer, "Analysis of variations of Volterra series models for RF power amplifiers," *IEEE Microw. Wireless Compon. Lett.*, vol. 23, no. 8, pp. 442–444, Aug. 2013.
[47] E. Zenteno, R. Piazza, M. R. B. Shankar, D. Rönnow, and B. Ottersten, "Multiple-input multiple-output symbol rate signal digital predistorter for non-linear multi-carrier satellite channels," *IET Commun.*, vol. 9, no. 16, pp. 2053–2059, Nov. 2015.
[48] Holzworth Instrumentation, "Ultra low phase noise—Phase coherent synthesizers," *Microw. J.*, no. 10, pp. 48–50, Aug. 2009.
[49] F. Gregorio, J. Cousseau, S. Werner, T. Riihonen, and R. Wichman, "Power amplifier linearization technique with IQ imbalance and crosstalk compensation for broadband MIMO-OFDM transmitters," *EURASIP J. Adv. Signal Process.*, vol. 2011, no. 1, p. 19, 2011.
[50] D. Astely, E. Dahlman, A. Furuskär, Y. Jading, M. Lindström, and S. Parkvall, "LTE: The evolution of mobile broadband," *IEEE Commun. Mag.*, vol. 47, no. 4, pp. 44–51, Apr. 2009.
[51] A. S. Tehrani, H. Cao, T. Eriksson, M. Isaksson, and C. Fager, "A comparative analysis of the complexity/accuracy tradeoff in power amplifier behavioral models," *IEEE Trans. Microw. Theory Techn.*, vol. 58, no. 6, pp. 1510–1520, Jun. 2010.
[52] J. G. Proakis and D. K. Manolakis, *Digital Signal Processing: Principles, Algorithms and Applications*, 3rd ed. Englewood Cliffs, NJ, USA: Prentice-Hall, 1996.
[53] E. Zenteno, Z. A. Khan, M. Isaksson, and P. Händel, "Using intrinsic integer periodicity to decompose the Volterra structure in multi-channel RF transmitters," *IEEE Microw. Wireless Compon. Lett.*, vol. 26, no. 4, pp. 297–299, Apr. 2016.
[54] E. Zenteno, Z. A. Khan, M. Isaksson, and P. Händel, "Finding structural information about RF power amplifiers using an orthogonal nonparametric kernel smoothing estimator," *IEEE Trans. Veh. Technol.*, vol. 65, no. 5, pp. 2883–2889, May 2016.

Zain Ahmed Khan (S'13) received the B.S. degree in electronics engineering from the Ghulam Ishaq Khan Institute, Topi, Pakistan, in 2005, and the M.S. degree in communication and signal processing from Technical University Ilmenau, Ilmenau, Germany, in 2013. He is currently pursuing the Ph.D. degree at the Department of Signal Processing, KTH Royal Institute of Technology, Stockholm, Sweden, where he involved in the behavioral modeling and digital predistortion of RF power amplifiers with a particular focus on MIMO transmitters.

He is currently with the Department of Electronics, Mathematics, and Natural Sciences, University of Gävle, Gävle, Sweden.

Efrain Zenteno (S'10–M'09) received the B.S. degree in electronics engineering from the Universidad San Agustn, Arequipa, Peru, in 2005, the M.Sc. degree in electronics and telecommunications from the University of Gävle, Gävle, Sweden, in 2008, and the Ph.D. degree from the KTH Royal Institute of Technology, Stockholm, Sweden, in 2015.

He is currently with the Electronics and Telecommunications Department, Universidad Catolica San Pablo, Arequipa, Peru, where he is responsible for teaching and research activities. His current research interests include measurements and signal processing for communications.

Peter Händel (S'88–M'94–SM'98) received the Ph.D. degree from Uppsala University, Uppsala, Sweden, in 1993.

From 1987 to 1993, he was with Uppsala University. From 1993 to 1997, he was with Ericsson AB, Kista, Sweden. From 1996 to 1997, he was a Visiting Scholar with the Tampere University of Technology, Tampere, Finland. From 2000 to 2006, he held an adjunct position with the Swedish Defence Research Agency. Since 1997, he has been with the KTH Royal Institute of Technology, Stockholm, Sweden, where he is currently a Professor of signal processing and the Head of the Department of Signal Processing. He has been a Guest Professor with the Indian Institute of Science, Bengaluru, India, and with the University of Gävle, Gävle, Sweden.

Dr. Händel was a recipient of a Best Survey Paper Award by the IEEE Intelligent Transportation Systems Society in 2013. He has served as an Associate Editor of the IEEE TRANSACTIONS ON SIGNAL PROCESSING.

Magnus Isaksson (S'98–M'07–SM'12) received the M.Sc. degree in microwave engineering from the University of Gävle, Gävle, Sweden, in 2000, the Licentiate degree from Uppsala University, Uppsala, Sweden, in 2006, and the Ph.D. degree from the KTH Royal Institute of Technology, Stockholm, Sweden, in 2007.

In 2012, he was a Docent in telecommunications with the KTH Royal Institute of Technology. From 1989 to 1999, he was with Televerket, Sweden, involved in communication products. Since 1999, he has been with the Department of Electronics, Mathematics, and Natural Sciences, University of Gävle, where he is currently a Professor of Electronics and the Department Head and also the Head of Research within the fields of mathematics and natural sciences. He has authored or co-authored many published peer-reviewed journal papers, books, and conference proceedings in these areas. His current research interests include signal processing algorithms for radio-frequency measurements and characterization, modeling, and compensation of nonlinear microwave devices and systems.